Eur. Phys. J. D **30**, 105–116 (2004)
DOI: 10.1140/epjd/e2004-00066-6

THE EUROPEAN PHYSICAL JOURNAL D

Trap loss rate for heteronuclear cold collisions in two species magneto-optical trap

M.W. Mancini, A.R.L. Caires, G.D. Telles, V.S. Bagnato, and L.G. Marcassa[a]

Instituto de Física de São Carlos, Universidade de São Paulo, P.O. 369, 13560-970 São Carlos, Brazil

Received 31 January 2003 / Received in final form 19 January 2004
Published online 11 May 2004 –

Abstract. In this paper we review the present status on heteronuclear trap loss rate (β') for alkali mixtures held in a magneto-optical trap (Na−K, Na−Rb, Na−Cs, K−Rb, Rb−Cs, Li−Cs). The intensity dependence of the β' for the mixture Cs−K is also presented for the first time in this report. The measurement techniques and a semiclassical model, considering both excited-ground and doubly excited channels, are reviewed. The comparison between the model and the experimental results indicates that radiative escape may be the dominant loss process for heteronuclear cold collisions. The obtained values for the crossed species trap loss indicate possibilities of future experiments involving such mixtures in a two species condensate.

PACS. 32.80.Pj Optical cooling of atoms; trapping – 33.80.Ps Optical cooling of molecules; trapping – 34.50.Rk Laser-modified scattering and reactions

1 Introduction

One of the main motivations in the development of atomic traps was the novel collisional regime which could be investigated. The new low energy collision makes a few effects, which are conventional negligible, remarkably important [1]. Since the collision partners have a de Broglie wavelength comparable to the typical interatomic potential range, the behavior of the atomic encounter is predominately quantum. In order to understand the experimental observations, a more elaborate model is necessary, especially if quantitative agreement is expected between experiment and theory. Another important fact is the collision time, which is either comparable or even greater than the excited-state lifetime. Therefore spontaneous emission can take place during the atomic encounter, affecting the overall collision results.

The Magneto Optical Trapping of atoms (MOT) is the most used tool in the field of cold atomic collisions [2,3]. In a MOT, atoms can be either in the ground-state or in the excited-state. This creates several possibilities for the atoms to start the atomic encounter. If both atoms are in their electronic ground-state during the whole collisional process, the influence of spontaneous emission is not present, and the system does not exchange energy with the light field. In this case, the main peculiarity of cold collision is the participation of very few partial waves in the process and its high dependence with details of the interatomic potential. In general, such collision are sensitive to external fields, for example, magnetic fields can severally affect the cross-section, even producing resonances in the elastic cross-section, the so-called Feshbach resonances [4]. There are two types of collisions involving an atomic pair in the ground-state. One of them is elastic scattering, which has a large variety of applications, for example evaporative cooling, collisions shift in high precision spectroscopy, and properties of a weakly-interacting Bose gas [5]. The other is the inelastic process; the nonzero nuclear spin of alkalis create a hyperfine structure for the ground-state and hence the possibility of hyperfine change collision (HCC) exists. This inelastic process which can occur during a ground-ground collision can, under some conditions, be the limiting factor for the number of trapped atoms [6].

If during the collision, one of the atoms is excited by the light field, the process can be classified as an excited-ground state collision. Involving an excited-state, the interatomic potential is predominantly of long range characterized by $1/R^3$ for the homonuclear case and $1/R^6$ for heteronuclear case. Due to the low energy of the collision, this long range potential can significantly affect the atomic encounter, even when the atoms are as far as $\lambda\!\!\!^{-}$ (the reduced wavelength of the light field) apart. Since the collisional times are comparable to the excited-state lifetime, spontaneous emission can take place during the atomic encounter, playing an essential role in the collision dynamics. The occurrence of spontaneous emission in this case causes a suddenly change of the molecular state together

[a] e-mail: marcassa@if.sc.usp.br

with the emission of a red-shifted photon, transferring the internal energy of the system to kinetic motion, resulting in a considerable increase of the atomic velocity. If the velocity is not too high, the viscous environment of the MOT is enough to dissipate it, allowing to the atoms to remain trapped. However, if the transferred kinetic energy is too high, atoms can be ejected from the trap. This constitutes an important trap loss mechanism referred to as radiative escape (RE). For alkalis there is also another exoergic process involving excite-ground collision. Due to the existence of the fine structure in the excited-state ($P_{3/2}$ and $P_{1/2}$), the atomic encounter can result in fine-structure-change (FSC) releasing energy, which is shared between both atoms in the form of kinetic motion. With this energy both atoms can easily escape from the MOT, which typically is $1K$ deep.

Over the past decade, many experiments have been devoted to the study of excited-ground state collisions using a sample of trapped cold atoms. In these binary homonuclear collision experiments, the three different exoergic processes described above have been observed for most of the alkalis [6,7]. They are the dominant effects for the loss mechanisms which prevent considerable increase in the maximum attainable density and number in these traps. For heteronuclear cold collisions the loss mechanisms are the same ones. However the internuclear long-range potential is weaker and shorter range interactions are more important. The dominant interaction term for the homonuclear ground-excited collisions depends on R^{-3}, while for heteronuclear collisions depends on R^{-6}. Thus the colliding atoms have to get much closer for the above mentioned loss processes effectively to take place. Therefore the probabilities of those mechanisms are considerably modified and within the laser cooling community it is important to identify and to understand the main physical processes involved in the two-species systems. Besides, several theoretical studies have recently been published, proposing a new series of experiments involving two different species of atoms trapped together: two species BEC [8] and ultracold photoassociative spectroscopy of heteronuclear molecules [9]. Recently, sympathetic cooling of mixtures of two different alkali species have been successfully used to achieve quantum regime. Bose-Einstein Condensation was simultaneously achieved in a mixture of bosonic species [10], as well as a degenerated Fermi regime in a Fermi-Bose mixture [11]. As in the case of single species, these experiments require high density samples. Therefore, an important step is the understanding and possible controlling of heteronuclear trap loss. In this context, the study of trap loss in a binary mixture comes at the right time and is significant first step for realization of these experiments. In this paper, we present a review on measurements of cross species trap loss rate for several systems (Na−K, Na−Rb, Na−Cs, K−Rb, Rb−Cs, Li−Cs) and we present for the first time the data and interpretation for the mixture Cs−K. We present a review on the measurement techniques, the adapted Gallagher-Pritchard model, and the comparison with experimental results.

2 Experimental set-up

Our mixed species MOT operates in a closed stainless steel vapor cell, and is loaded with the slowest atoms of a Maxwellian velocity distribution from the gas. Details about the vapor cell MOT operation has already been described elsewhere [6]. A peculiarity of our cell is that it contains separate reservoirs for sodium, potassium, rubidium and cesium that were assembled in a 6 way cross on one arm of the main chamber. Each reservoir has an independent control for temperature and a valve that provide the desired flux of atoms from the picked species to be trapped. The background pressure inside the cell is kept to about 10^{-9} Torr, which is obtained using a combination of turbo-molecular and ion pumps. The control of partial pressures (via the reservoir temperature) is important because of the considerably different vapor pressures of the various alkalis when at the same temperature. If the partial pressures are too different the excessive background vapor of one species may compromise the performance of the other species trap [12,13]. Similar experimental setups were used to study Li–Cs [14] and Na–Cs [15].

A combination of several dye, Ti:sapphire and diode lasers were used to trap the different atomic species. In the xy-plane of the chamber plane there are two independent counterpropagating laser beams entering the vapor cell for each species. In the z-axis the species A and species B laser beams are combined in a dichroic mirror. Circular polarized light in the xy-plane is produced by $\lambda/4$ plates for each species and by Fresnel rhombus in the z-axis. This scheme of independent optics for each atomic species guaranteed a very good control of the spatial overlap for the two trapped atomic clouds which is essential for collision experiments. The number of trapped atoms of both species were determined by imaging their fluorescence onto a calibrated photomultiplier tube (PMT), while their dimensions were measured with a charge-coupled device camera (CCD) using passband optical filters. The atomic densities were obtained using these parameters. In Table 1 we present the trap parameters (detuning, laser intensity) as well the individual trapped densities and total numbers of atoms for most of the experiments here reported. The listed total number of atoms and their density presented here for each species represent values in the absence of the other species.

3 Measurement techniques of the cross species trap loss rate

The loading process for the atomic species A in the presence of the atomic species B is given by the following rate equation:

$$\frac{dN_A}{dt} = L - \gamma N_A - \beta \int_{v_A} n_A^2 d^3r - \beta' \int_{v_A} n_A n_B d^3r \quad (1)$$

where L is the loading rate for the species A, γ is the loss rate caused by collisions between the trapped atoms of species A and the hot background gas (which is composed

Table 1. Trapping laser parameters (detuning and intensity), total number of trapped atoms (N) and atomic density (n) for the heteronuclear trap loss experiments [10–15]. The listed total number of atoms and their density presented here for each species represent values in the absence of the other species.

Colliding species	^{23}Na+^{39}K [10]	^{23}Na+^{85}Rb [11]	^{7}Li+^{133}Cs [12]	^{23}Na+^{133}Cs [13]	^{39}K+^{85}Rb [14]	Rb+^{133}Cs [15]	^{23}Na+Rb [16]
Δ_A	$-\Gamma_{\rm Na}$	$-\Gamma_{\rm Na}$	$-[1,6]\Gamma_{\rm Li}$	$-\Gamma_{\rm Na}$	$-7\Gamma_{\rm K}$	$-\Gamma_{\rm Rb}$	$-1.4\Gamma_{\rm Na}$
Δ_B	$-7\Gamma_{\rm K}$	$-2\Gamma_{\rm Rb}$	$-[1,5]\Gamma_{\rm Cs}$	$-4\Gamma_{\rm Cs}$	$-2\Gamma_{\rm Rb}$	$-2\Gamma_{\rm Cs}$	$-3.7\Gamma_{\rm Rb}$
$I^{\rm A}_{tot}$(mW/cm^2)	$0.5-2.0$	$20-150$	47	$10-200$	$70-110$	$10-250$	$10-100$
$I^{\rm B}_{tot}$(mW/cm^2)	150	230	26	$10-200$	230	$40-400$	15
N_A(atoms)	10^6	10^6	10^9	10^6	10^9	10^8	10^6
N_B(atoms)	10^8	10^8	10^6	10^7	10^9	10^7	10^6
n_A(atoms/cm^3)	1.3×10^{10}	2×10^{10}	10^{10}	10^{10}	1.5×10^{10}	10^{10}	3×10^9
n_B(atoms/cm^3)	8.5×10^9	4×10^{10}	10^{10}	10^{10}	2×10^{10}	10^{10}	3×10^9

mostly by thermal A and B species atoms), β is the loss rate resulting from collisions among the trapped atoms of species A, β' is the loss rate due to cold collisions between trapped atoms of species A and B, N_A is the number of trapped atoms of species A, n_A and n_B are the density profiles of both species A and B respectively. We have to emphasize that β' should be read as $\beta'_{\rm A-B}$, unless mentioned. This subindex arrangement, A−B, is in order to indicate that the first species is the one in which the losses are been observed when the second species is present. The integration in equation (1) is performed over the whole volume occupied by the atoms of species A. For Gaussian spatial distributions, $(n_A(r,t) = n_{0A}(t)e^{-2(r/w_A)^2}$ and $n_B(r,t) = n_{0\rm Rb}(t)e^{-2(r/w_B)^2})$, equation (1) can be rewritten as:

$$\frac{dN_A}{dt} = L - \left[\gamma + \beta' N_B \left[\frac{2(w_A^2+w_B^2)}{(w_A w_B)^2\pi}\right]^{3/2}\right] N_A - \beta\left(\frac{4}{w_A^2\pi}\right)^{3/2} N_A^2. \quad (2)$$

One may notice that if we have chosen the species B atoms to study, equation (1) would be identical, except for the B subindexes, but we will be interested in measuring a $\beta'_{\rm B-A}$ rate coefficient. However, in principle there should be no reason why the $\beta'_{\rm B-A}$ will be reciprocal to that one in the A sample, $\beta'_{\rm A-B}$. This is justified if one think about, for example, the different C_6 coefficients involved in all possible collision channels in each situation, and also the trap depths for each MOT are not equal and may change for different trapping conditions.

There are two techniques to measure β', they are called the **differential method** and the **remaining number of trapped atoms method**. The **differential method** consists of a two steps procedure to determinate β' [12,13]. We first block one arm of the species B trap laser, avoiding the formation of the cold cloud of species B while leaving most of the laser light on. In this situation $n_B = 0$ and the term containing β' in equation (2) drops out. We observed the loading process of the species A atoms with a PMT. The number of the trapped atoms is obtained from the PMT signal and the dimensions from the CCD camera images. Using the calculated atomic density we can obtain the rates γ and β by fitting the loading curves using $n_{\rm Rb} = 0$ (Eq. (2)). Second, the species B trap arm was unblocked, allowing the complete formation of species B cloud, and we again observed the loading process for species A. In Figure 1a we show the loading process. Both clouds were then observed and measured. Finally we fitted the loading curve with the solution of equation (2) and obtained the rate β', using γ and β values previously measured.

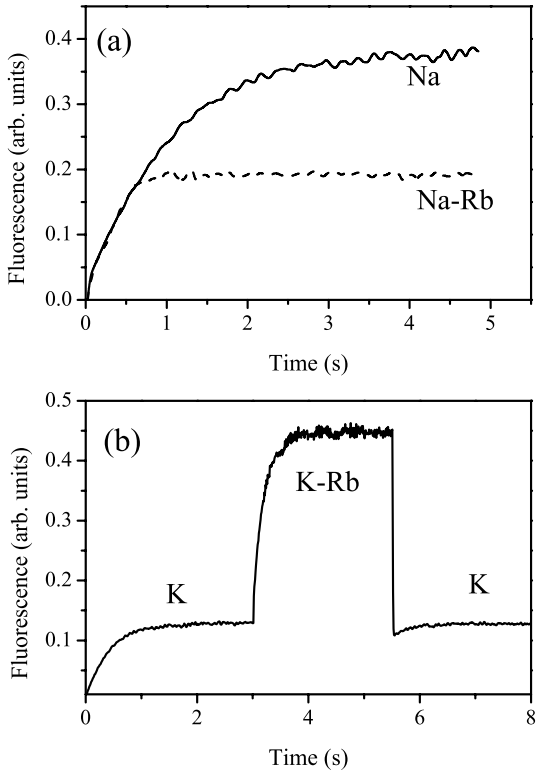

Fig. 1. (a) Typical loading curve using the differential method in a sample of Na–Rb. (b) Typical loading curve using the remaining number of trapped atoms method in a sample of K–Rb.

The **remaining number of trapped atoms method** consists of three steps [16]. The experiment begins by blocking one arm beam of each MOT to prevent any kind of species from being trapped. The species A arm beam is then unblocked. By imaging its fluorescence

onto a calibrated photomultiplier, we obtain the transient loading curve and the steady state number of the trapped atoms for species A. After the species A MOT reaches its steady state number, its volume can be characterized by taking a picture with a charge-coupled device camera (CCD). In the second step, the species B trap is allowed to be formed, and we observe its loading process through the same photomultiplier that was used to observe the species A fluorescence. Thus, sufficient time elapses for the species B trap to reach a steady state. A new image of the combined trap is shot by the camera. After the species B MOT is suddenly emptied (by blocking the species B trap light), the number of trapped species B is determined though the variation of the PMT signal. At this point, a new picture of the remaining species A trap is taken and its steady state number (in the presence of species B) is also determined. The above described procedure allows us to define the total number of remaining trapped atoms for species A and the dimensions of the sample when cold sample of species B was present. The last step takes under 3 ms, which is insufficient time for the species A cloud to change, thus preserving its final form and number while in the presence of species B. Finally, we check the recovery of the species A MOT (number of atoms and density) to ensure stability throughout the procedure, which is indicated by its full recovery. This technique is similar to the differential method and its loading process is shown in Figure 1b.

During the first step, $N_B = 0$, we can, therefore, extract γ, β and the final steady state number of trapped atoms for species A, N_A^F from the loading data. In the second step, the drop in fluorescence allows one to determine the number of trapped atoms of species B in the steady state (N_B^F) as well as the number of trapped atoms of species A in the presence of cold sample of species B, which decreases in relation to the number that we originally started with. The dimensions of the species A and B samples can be obtained using the pictures of the sample framed during the entire procedure. β' is then calculated using all this information plus the steady state solution of equation (2). We have observed that the data obtained by this technique presents considerably less fluctuations in comparison to the previous technique employed by our group [12,13], and we ascribe this to the fact that this new technique requires less time for data acquisition. Hence, this technique is less sensitive to long term variations of trap conditions.

4 The adapted Gallagher-Pritchard model for the cross species trap loss rate

In a heteronuclear atomic sample there are three possible loss channels for exoergic cold collisions, which depend on the combination of the levels of the colliding atoms: (i) both atoms in the ground state; (ii) one atom in the excited state and the other in the ground state; (iii) both atoms in the excited state. For the excited-ground state collision, there are two possibilities to be considered, i.e., either atom A is excited and atom B is the ground state or atom A is in the ground state while atom B is excited. Each of those channels present different interaction potentials; the ground-ground and excited-ground states present a C_6/R^6 potential, while the excited-excited case presents a C_5/R^5 potential. It is difficult to identify the main loss channel simply by comparing the potentials. Therefore, in order to understand the results and to determine the contribution of each channel to the total cross species loss, we have constructed simple models that can provide us with the relative contribution of each channel. Owing to its simplicity and the fact that it provides numerous physical insights, we will use a semiclassical model normally referred to as the Gallagher-Pritchard (GP) model [19]. We will apply this model to a heteronuclear excited-ground state collision with a C_6/R^6 potential. To calculate the contribution of the excited-excited state collision, we will modify the model proposed by Gallagher [20] for photoassociative ionization in sodium in order to account for the mechanisms involving *two color* trap loss. We should point out that, as a first approach, only the radiative escape (RE) loss mechanism was considered. This approach is justified on the basis of recent experimental results, in which the RE appears to be the dominant mechanism for the trap loss rate [21–23].

For the excited-ground state loss channel contribution, the following steps were considered [16]. First, the A–B pair absorbs a photon and goes to the attractive potential. In this step any of the two atomic species (A and B) may be excited by either of the photons ν_A or ν_B, this depends on the existence of attractive potentials. Here we will describe the case where the atomic species A is excited. The colliding pair may decay during the collision, emitting a photon to the red of the atomic transition ($h\nu$). The energy difference goes to kinetic energy (ΔE_{K}) and it will be shared between the atoms according to their mass ratio (m_A/m_B); if the energy is sufficient, either both atomic species will escape from the MOT's or just the lighter. This process can be described as follows (Fig. 2a):

$$\mathrm{A}(\mathrm{S}_{1/2}) + \mathrm{B}(\mathrm{S}_{1/2}) + h\nu_A \rightarrow \mathrm{A}^* - \mathrm{B} \rightarrow \mathrm{A}(\mathrm{S}_{1/2}) + \mathrm{B}(\mathrm{S}_{1/2}) + h\nu + \Delta E_{\mathrm{K}}. \quad (3)$$

In this case, the model is implemented taking into account the number of atomic pairs between R_0 and $R_0 + dR_0$ that can are excited by the laser and be able to survive until short internuclear separation (where radiative escape takes place). To account for every possible internuclear separation, an integration is performed. As an example, the loss rate (β'_*) for the A*–B channel is written as:

$$\beta'_* = \frac{1}{2}\int_0^\infty 4\pi R_0^2 \epsilon_A(R_0, \omega_A, I_A) P_{RE}(R_0, v_{esc}) dR_0 \quad (4)$$

where $\epsilon_A(R_0, \omega_A, I_A)$ is the excitation rate of species A, which depends on R_0, on the frequency (ω_A) and on the intensity (I_A) of the species A laser; $P_{RE}(R_0, v_{esc})$ is the probability that RE will occur, which depends on R_0 and the escape velocity (v_{esc}) of the atomic species in which the loss occur. Here we will consider that we are observing

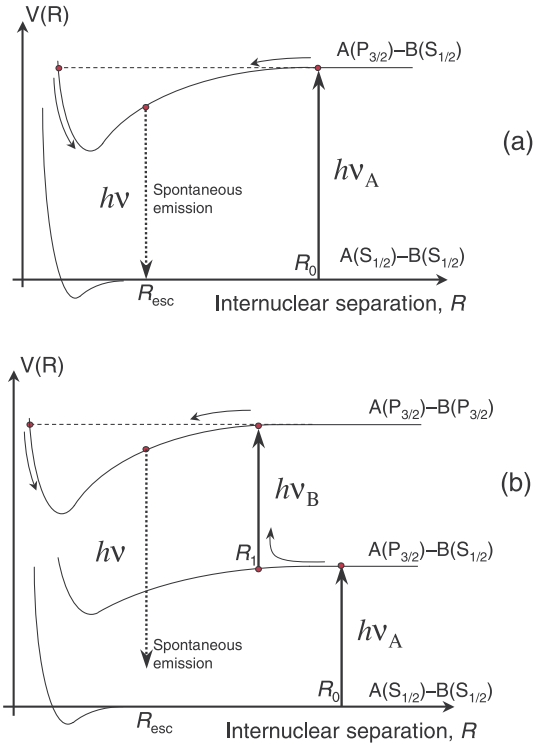

Fig. 2. (a) Schematic diagram showing the A*–B loss channel; (b) schematic diagram showing the A*–B* loss channel.

the losses in species A. Therefore β'_* is the "cross species loss rate" in species A due to collisions in species B. In the heteronuclear case we have the excitation probability rate as:

$$\epsilon_A(R_0,\omega_A,I_A)=\frac{(\Gamma_A/2)^2}{(\omega_A-\omega_{A0}+C_6/R_0^6)^2+(\Gamma_A/2)^2}\times\frac{I_A}{h\omega_A}\frac{\lambda_A^2}{2\pi} \quad (5)$$

and

$$P_{RE}(R_0,v_{esc})=\frac{\sinh[\Gamma_A t^*(R_0,v_{esc})]}{\sinh(\Gamma_A T^*(R_0))} \quad (6)$$

where Γ_A and ω_{A0} are the natural linewidth and resonance frequency for the A atom; λ_A is the wavelength of the A laser; $t^*(R_0,v_{esc})$ is the time spent in the region where RE occurs, and $T^*(R_0)$ is the time for the pair to go from $R=R_0$ to $R=0$. If a classical motion for the atomic pair in the A*–B potential is considered, these times can be expressed easily in terms of R_0 and v_{esc}. It is important to point out that $P_{RE}(R_0,v_{esc})$ is proportional to $1/v_{esc}^{4/3}$ and this is an important parameter in our model. To calculate it we have used a one dimensional model in which the radiative forces are considered based on the Doppler theory [24]. As pointed out by Wallace et al. [7] the velocity dependent dissipative force dominates over the position dependent restoring force, therefore the escape velocity is mainly determined by the damping coefficient. According to reference [1], the escape velocity can be expressed as $v_{esc}=\alpha w/m$ (where α is the damping coefficient, w is the laser beam waist and m is the atomic mass). This, in fact, is confirmed by a recently experiment done by our group [25]. In that work we have measured the intensity dependence of the capture velocity of the atoms in a sodium MOT. The experimental results were compared with a simple three-dimensional simulation model where the radiative forces involved in the trap due to all the lasers beams are considered within the Doppler theory. It was considered the anisotropy of the trap and averaging over all the possible directions to obtain the capture velocity. This procedure is similar to the one discussed in reference [26]. With this model, we can reproduce well the experimental results for the measured capture velocity. It also predicts the same intensity dependence for the escape velocity, but with smaller values than the capture velocity. The damping model also agrees with the complex model for the intensity dependence of the escape velocity and give us confidence to use such model.

For the contribution of the excited-excited state loss channel, we have considered the following sequential process [16]. The colliding pair A–B absorbs a photon ($h\nu_A$) at R_0 and goes to the attractive potential (A*–B), acquiring some kinetic energy while in this potential. The system then absorbs the second photon ($h\nu_B$) at R_1, going to the excited-excited potential. In this potential, the pair reaches the short range, where it emits a photon to the red of the atomic transition ($h\nu$). The energy difference is shared between the A and the B atoms. This process can be described, as shown in (Fig. 2b), by:

$$\begin{aligned}\mathrm{A(S_{1/2})+B(S_{1/2})}+h\nu_A\rightarrow \mathrm{A^*-B}+h\nu_B\rightarrow \mathrm{A^*-B^*}\\ \mathrm{A^*-B^*}\rightarrow \mathrm{A(S_{1/2})+B(S_{1/2})}+h\nu+\Delta E_{\mathrm{K}}.\end{aligned} \quad (7)$$

Here we will consider the decay of the A*−B* in only one step for simplicity of the model. This is reasonable due to the short lifetime of such states and the lack of resonant photons to re-excite the system to the A*−B*. We do not believe that such simplification will be important in the model. For this case, the cross species trap loss rate (β'_{**}) in species A due to collisions with species B is given by:

$$\beta'_{**}=\frac{1}{2}\int_0^\infty\int_0^{R_0}4\pi R_0^2\epsilon_A(R_0,\omega_A,I_A)P_S(R_0,R_1)\times\epsilon_B(R_1,\omega_B,I_B)P_{RE}(R_0,R_1,R_{esc})\frac{dR_1}{v(R_0,R_1)}dR_0 \quad (8)$$

where $\epsilon_A(R_0,\omega_A,I_A)$ is the excitation rate for the first photon absorption (which is equal to Eq. (6)); $P_S(R_0,R_1)$ is the probability that the atomic pair will not decay or undergo a RE process while in the A*–B potential; $\epsilon_B(R_1,\omega_B,I_B)$ is the excitation rate for the second photon absorption (the $1/R^5$ potential of the excited-excited state and the $1/R^6$ potential of the excited-ground state are taken into account); $v(R_0,R_1)$ is the velocity of the pair at R_1; $dR_1/v(R_0,R_1)$ is the transit time in the region of the second absorption; and $P_{RE}(R_0,R_1,R_{esc})$ is the probability that a RE will take place while in the excited-excited potential. The excited-excited heteronuclear case

can be expressed as follows:

$$P_S(R_0, v_{esc}) = \frac{\exp[-\Gamma_A \Delta t^*(R_0, R_1)]}{1 - \exp(-2\Gamma_A T^*(R_0))} \quad (9)$$

$$\epsilon_B(R_1, \omega_B, I_B) = \frac{(\Gamma_B/2)^2}{(\omega_B 8 - \omega_{B0} + C_5/R_1^5 - C_6/R_1^6)^2 + (\Gamma_B/2)^2} \frac{I_B}{h\omega_B} \frac{\lambda_B^2}{2\pi} \quad (10)$$

$$P_{RE}(R_0, R_1, v_{esc}) = \frac{\sinh[\Gamma_B t_1^*(R_0, R_1, v_{esc})]}{\sinh(\Gamma_B T_1^*(R_0, R_1))} \quad (11)$$

where $\Delta t^*(R_0, R_1)$ is the time for the pair to go from $R = R_0$ to $R = R_1$, $T_1^*(R_0, R_1)$ is the time for the pair to go from $R = R_1$ to $R = 0$ and $t_1^*(R_0, R_1, v_{esc})$ is the time spent in the region where RE occurs in the excited-excited potential.

It is important to point out that in this section we have consider particular atomic excitations for both channels; and we only consider the losses occurring in the species A due to species B. One may extent this to other possibilities, where either the species B is the first to be excited or the loss occur in species B. In any case, it will be just an extension of the model here proposed. We should point out that these are the simplest models that one may consider. Some important effects as temperature dependence of relative velocity [14], shielding [27] as well as flux enhancement [28] were not considered within such models.

5 Results and discussion

Each combined species system presents its own peculiarity and they will be individually present as follow.

5.1 System Na–K

In Figure 3 we show the dependence of β' observed in Na atoms due to collisions with K atoms as a function of sodium laser intensity (I_{Na}); the data were extracted from reference [29]. The authors of reference [29] associated the raising up at low intensity with the occurrence of heteronuclear hyperfine changing collision (HHCC) because they worked in an intensity regime well below saturation. Due to this fact they did not consider others collisional mechanisms, as radiative escape (RE) and fine structure changing collisions (FSC), to explain the observed results. In fact, the FSC mechanism can be excluded because the authors did not observed any loss in the K atoms when the Na atoms were introduced. In a heteronuclear system the fine structure can happen in either atoms in both channels (Na*–K* and Na–K*). The FSC in sodium and in potassium will release 12 K and 104 K of energy respectively. In any case both atoms (Na and K) of the colliding pair will gain enough energy to escape from the trap. Therefore, if FSC was the dominant loss process in heteronuclear collisions we should measured similar losses in sodium and potassium. However, the experiment of reference [29] showed that the potassium MOT is not affected by the presence of the sodium MOT ($\beta'_{\mathrm{K-Na}} \lll \beta'_{\mathrm{Na-K}}$), and therefore we can excluded FSC.

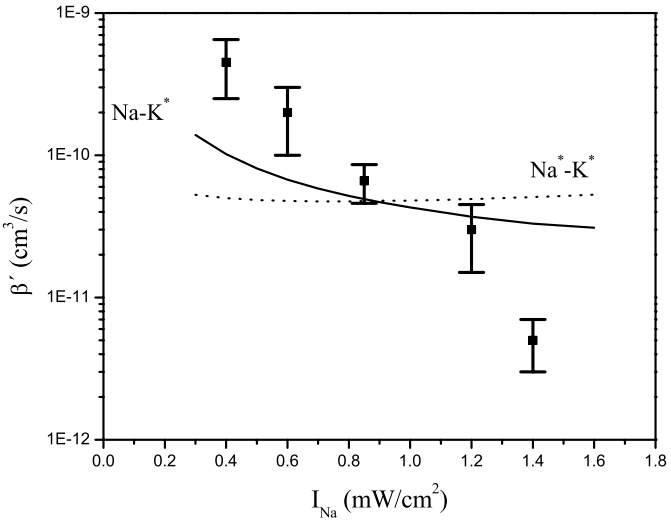

Fig. 3. Intensity dependence of the heteronuclear trap loss rate for Na atoms as a function of sodium trapping laser intensity in the presence of K [10]. The predictions for the two possible collisional channels, Na−K* and Na*–K*, are represented by solid and dashed lines respectively.

If we applied the models proposed in the previous section, which considers the radiative escape mechanism, we can obtain their predictions for the two possible collisional channels, Na−K* and Na*–K*, which are represented by solid and dashed lines respectively in Figure 3. For the mechanisms involving Na*–K* the model predicts a weak intensity dependence (Fig. 3 – dashed line), a stronger dependence is predicted for the Na−K* case (Fig. 3 – full line). Because of the difference in the intensity dependence, we believe that the main contribution to β' comes from collisions involving Na−K*. As the intensity goes down, the Na trap depth decreases but the population of excited K is kept constant producing an increase in β'.

5.2 System Na–Rb

In Figure 4, we show the dependency of β' observed in Na atoms due to collisions with Rb atoms as a function of sodium laser intensity (I_{Na}) [13]. To understand the behavior of the experimental points for β', we have separately considered the contribution of Na−Rb* and Na*–Rb* channels and the RE mechanism. The results are shown in Figure 4 as full and dashed lines respectively. For the mechanisms involving the Na*–Rb* channel the model predicts a weaker intensity dependence than for the Na−Rb* case. We believe that the saturation of the Na*–Rb* channel is due to the saturation in the excited state population. On the other hand, the intensity dependence of β' due to the Na−Rb* channel comes from the fact that as the intensity goes down, the Na trap depth decreases but the population of excited Rb is kept constant producing an increase in β'.

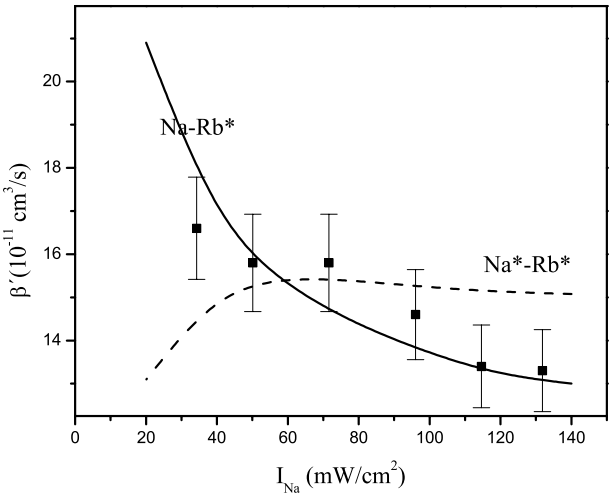

Fig. 4. Intensity dependence of the heteronuclear trap loss rate for Na atoms as a function of sodium trapping laser intensity in the presence of ^{85}Rb [11]. The predictions for the two possible collisional channels, Na−Rb* and Na*–Rb*, are represented by solid and dashed lines respectively.

Similar results for β' were observed by Young and co-workers [18], but the authors associated the observed behavior with the occurrence of heteronuclear hyperfine changing collision. If we applied the adapted GP model considering both channels and RE, we are able to reproduce quite well the experimental results. In Figures 5a and 5b we show the experimental results of reference [18] and our model predictions for collisions involving ^{85}Rb and ^{87}Rb samples respectively. We should point out that in both experiments [13,18], the authors did not observed any influence on the Rb MOT due to the presence the Na MOT. This fact exclude the occurrence of heteronuclear fine structure changing collisions because the energy involved in this process is larger than any trap depth, as explained before.

In the study of excited-ground state collisions within cold atoms, the rate variation of the loss rate with the laser frequency is important and provides additional information about excitation occurring at different internuclear separations. Also this kind of data allows one to observe the important role of spontaneous emission in the process. Normally, the investigation of the loss rate dependence on detuning is done using the technique named "optical catalysis" [30]. It consists in adding an extra laser to the system, whose frequency is scanned, introducing extra collisional losses (reducing the total number of trapped atoms). To obtain information about the dependence of β, or β', with the detuning one has to keep the number of atoms constant, for each laser frequency, while the intensity of the extra laser ("catalysis laser") is adjusted. If $I_c(\Delta)$ is the intensity required to keep N, then $\beta(\Delta) \propto 1/I_c(\Delta)$, as demonstrated in reference [30]. To ensure reliability of this procedure a special care must be taken to verify that the "catalysis laser" is not affecting the optical pumping rate, the loading rate, and it is not causing extra force on the atomic cloud.

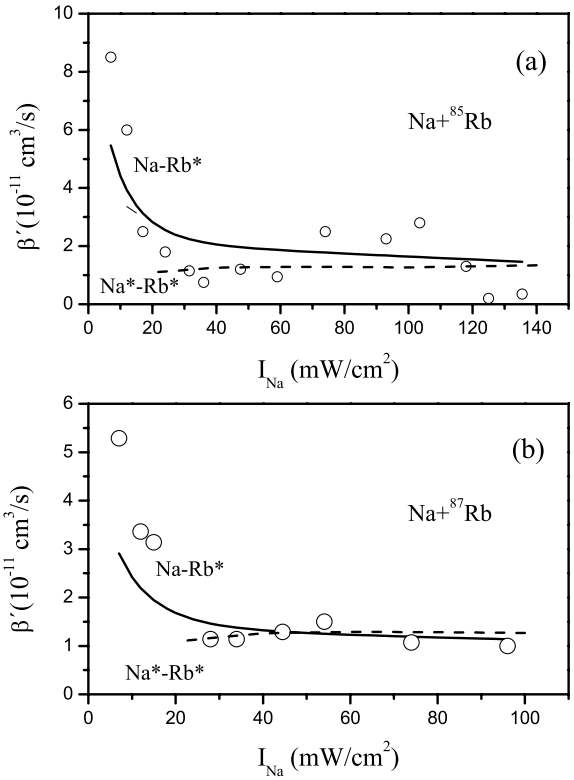

Fig. 5. Intensity dependence of the heteronuclear trap loss rate for Na atoms as a function of sodium trapping laser intensity in the presence of: (a) ^{85}Rb; (b) ^{87}Rb [13]. The predictions for the two possible collisional channels, Na−Rb* and Na*–Rb*, are represented by solid and dashed lines respectively.

For our experimental conditions, we verified that for the catalysis laser frequency closer than −70 MHz from the atomic resonance, the trapping performance was affected. Therefore we restricted ourselves to a detuning range from −100 to −1000 MHz. It is worth to mention that in a two species MOT the extra laser will increase both the homonuclear and the heteronuclear collisions. Thus, at this time we did not measure any specific catalysis loss rate, β_c or β'_c, but a total loss, β_{Tc}, which is a combination of these two rates.

The obtained dependence for the total catalysis loss rate, β_{Tc}, as a function of detuning is presented in Figure 6. The logarithmic plot reveals that the dependence for the catalysis experiment is $\beta_{Tc} \propto \Delta^{-2\pm0.2}$. This result is different from that for Na only, $\beta_c \propto \Delta^{-7/6}$, correctly predicted the Gallagher-Pritchard (GP) model [19] when a C_3/R^3 attractive potential is considered. In a first attempt we have modified the homonuclear GP model by simply changing the internuclear asymptotic dependence, introducing the C_6/R^6 attractive potential, which is the dominant coefficient for the heteronuclear long range interacting potential. The result for the loss rate was $\beta'_c \propto \Delta^{-5/6}$, which is still far from that experimentally observed dependence. But, in a recent paper [31] we were able to reproduce this observation relying on the Na*–Rb* channel, this prediction is represented by a full line in Figure 6.

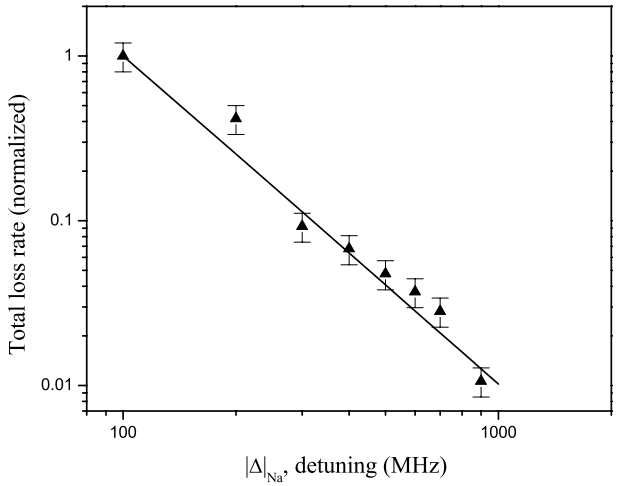

Fig. 6. Total loss rate in Na plotted as function of the sodium detuning. The theoretical heteronuclear loss rate as function of the detuning, predicted by the double excited model is presented as solid line.

5.3 System Na–Cs

In Figure 7 the dependence of β' observed in Na atoms due to collisions with Cs atoms is shown as a function of sodium laser intensity (I_{Na}) (Fig. 7a) and as a function of cesium laser intensity (I_{Cs}) (Fig. 7b). The data were extracted from reference [15]. The authors of reference [15] associated the observed loss in Na sample with the occurrence of heteronuclear hyperfine structure changing collision in sodium atoms. The FSC in sodium will release 12 K of energy and the Cs atom will gain more than 2 K, which is more than enough to make it to escape from the trap. Therefore, if FSC was the dominant loss process in heteronuclear collisions the authors of reference [15] should measured similar losses in sodium and cesium. However, they did not observe any variation in the Cs trap ($\beta'_{\mathrm{Cs-Na}} \lll \beta'_{\mathrm{Na-Cs}}$). This is a strong indication that FSC is not important in this system and radiative escape has to be the dominant process. We also show the theoretical prediction considering the $\mathrm{Na}^*-\mathrm{Cs}^*$ channel (dashed line) and $\mathrm{Na}-\mathrm{Cs}^*$ channel (full line) in Figure 7.

5.4 System K–Rb

In Figure 8 we show the dependence of β' observed in K atoms due to collisions with Rb atoms is shown as a function of potassium laser intensity (I_{K}). These data were obtained in our previous work [16]. In this figure we also show the normalized model's predictions as a function of laser intensity (dashed line for K–Rb^* and full line for K^*–Rb^*, respectively). Using the experimental procedure described herein, we cannot separate the individual contribution of each possible collisional process. However, we can observe that the K^*–Rb^* channel presents a stronger intensity dependence than the K–Rb^* channel, which agrees better with the experimental results. In this work, we also had tried to explain the increase in β' at the low intensity

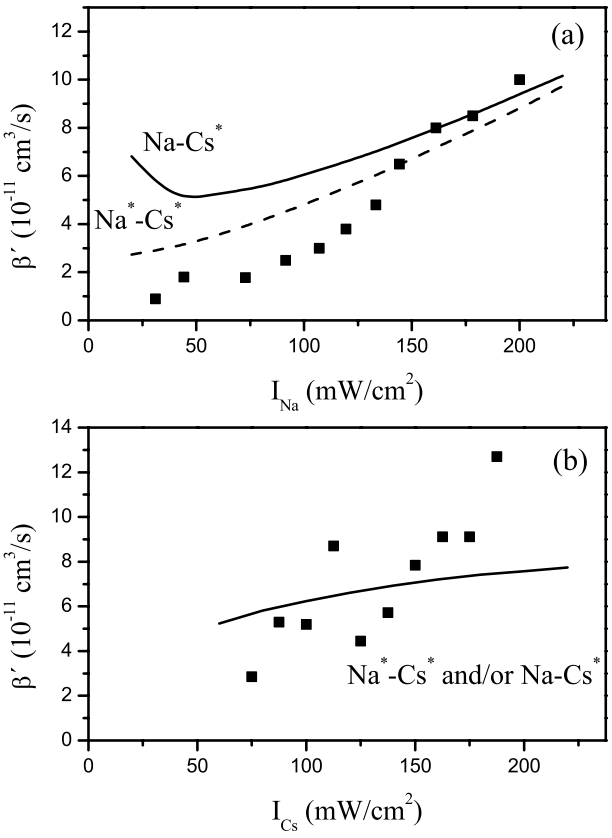

Fig. 7. Intensity dependence of the heteronuclear trap loss rate for Na atoms in the presence of ^{133}Cs as a function of: (a) sodium trapping laser intensity. The predictions for the two possible collisional channels, $\mathrm{Na}-\mathrm{Cs}^*$ and $\mathrm{Na}^*-\mathrm{Cs}^*$, are represented by solid and dashed lines respectively; (b) cesium trapping intensity. Both channels prediction the same intensity dependence (solid line).

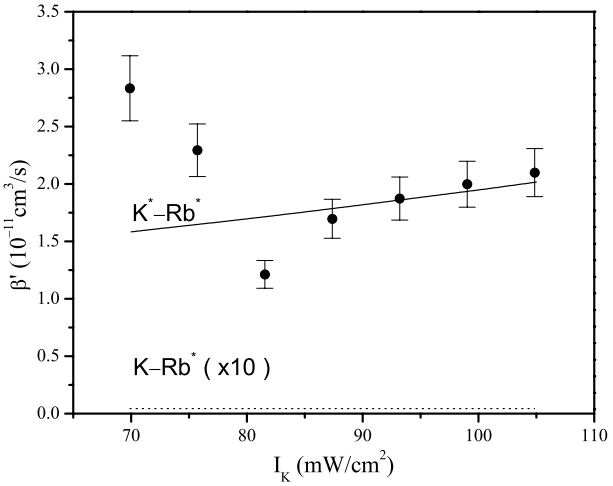

Fig. 8. Intensity dependence of the heteronuclear trap loss rate for K atoms in the presence of ^{85}Rb as a function of potassium trap laser intensity. The dashed line is the model's prediction for the K–Rb^* channel and the full line for the K^*–Rb^* channel, respectively.

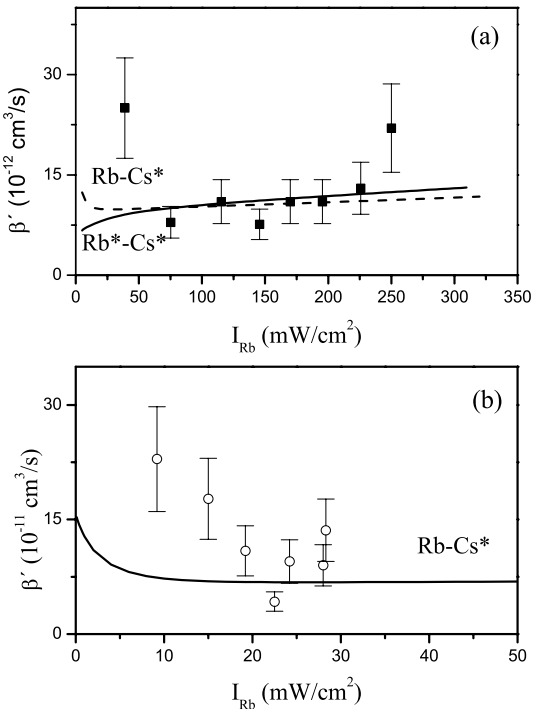

Fig. 9. Intensity dependence of the heteronuclear trap loss rate for Rb atoms in the presence of ^{133}Cs as a function of: rubidium trapping laser intensity: (a) the squares points refer to the data from the B-experiment. The predictions for the two possible collisional channels, Rb−Cs* and Rb*–Cs*, are represented by dashed and solid lines respectively; (b) the hollow circles report the data from the I-experiment. The Rb−Cs* channel seems to be the only capable to reproduce the experimental observations of the I-experiment. This figure has to be looked at with care, remembering that both experiments have been done in different conditions.

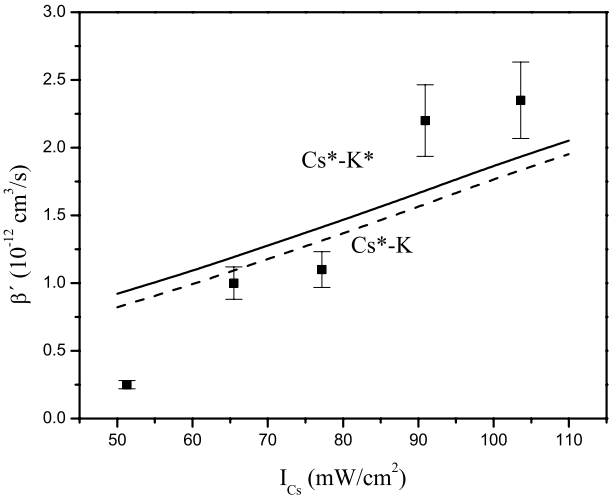

Fig. 10. Intensity dependence of the heteronuclear trap loss rate for Cs atoms in the presence of ^{39}K as a function of cesium trapping laser intensity. The predictions for the two possible collisional channels, Cs*–K and Cs*–K*, are represented by a solid lines.

regime due to Heteronuclear Hyperfine Changing Collision (HHCC). But, we also observe that the adapted GP model considering the K*–Rb* channel presents a raising up at low intensity, which is due to the intensity dependence of the potassium escape velocity as pointed out by Telles et al. [32]. This may be an alternative explanation for the behavior observed at low intensity.

We should point out that in our experiment the rubidium MOT was not affected by the presence of the potassium MOT ($\beta'_{\mathrm{Rb-K}} \lll \beta'_{\mathrm{K-Rb}}$). This is a strong indication that FSC is not important in this system and radiative escape has to be the dominant process.

5.5 System Rb–Cs

Figure 9 reports the measured values for the Rb loss rate due to heteronuclear collisions with Cs, β', versus the rubidium trap laser intensity (I_{Rb}) for experiments carried out in Brazil (B-experiment, Fig. 9a) and in Italy (I-experiment, Fig. 9b) [17]. The result from the B-experiment refer to the ^{85}Rb data, while the I-experiment refer to the ^{87}Rb data. The data of Figure 9 shows at low trap laser intensities a very large change in the absolute β' values. On the contrary, a small variation of β' was observed when the laser intensity increased. The overall change of β' is roughly one order of magnitude, in agreement with the change measured in other measurements of the loss rate β' for heteronuclear alkali collisions. We were able to observe that $\beta'_{\mathrm{Cs-Rb}}$ is 20 times smaller than $\beta'_{\mathrm{Rb-Cs}}$, showing a non reciprocity for β'; and therefore excluding FSC as a loss mechanism.

To analyze the dependence of β' on the laser intensity, we have considered two possible mechanism, Rb−Cs* and Rb*–Cs*. In Figure 9a, we plotted the model's prediction for the Rb−Cs* channel (as a dashed line) and Rb*–Cs* channel (as a full line). From the B-experiment we have the impression that the Rb*–Cs* channel represent well the observed behavior of β' at high intensity regime. At low intensity, the Rb−Cs* represents better the behavior of β'. In Figure 9b, this channel seems to be the only capable to reproduce the experimental observations of the I-experiment.

5.6 System Cs–K

Figure 10 reports the measured values for the Cs loss rate due to heteronuclear collisions with K, β', versus the cesium trap laser intensity (I_{Cs}). The data shows that the β' increases as the laser intensity increases, which suggests that the cesium excited state population is an important parameter for the heteronuclear trap loss rate. We should point out that we were not able to measure the K loss rate due to heteronuclear collisions with Cs; because the Cs MOT was much smaller than the K MOT, therefore the number of trapped K atoms colliding with Cs atoms too small to be detect.

To analyze the dependence of β' as a function of the cesium laser intensity, we have considered two possible

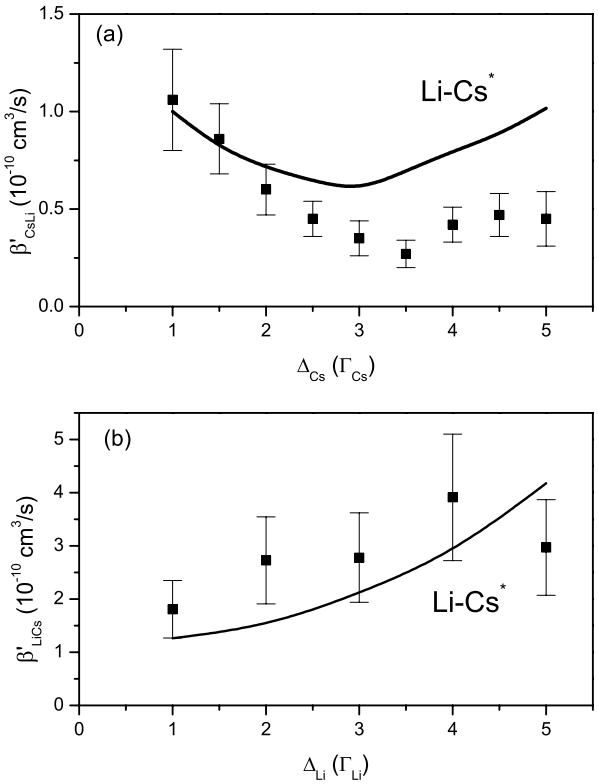

Fig. 11. (a) Trap loss rate of Cs atoms in the presence of Li (β'_{CsLi}) as a function of Δ_{Cs}; (b) trap loss rate of Li atoms in the presence of Cs (β'_{LiCs}) as a function of Δ_{Li}. The predictions for the two trap loss rates, considering radiative escape in the Li−Cs*, are represented by a solid lines.

mechanism, Cs*–K and Cs*–K*. In Figure 10, we plotted the model's prediction for the Cs*–K channel (as a dashed line) and Cs*–K* channel (as a full line). Both channels predict the same intensity behavior in the studied intensity interval. This is due to the fact that our escape velocity model for cesium MOT does not present a strong intensity dependence in this interval. Therefore, β' is basically dependent only on the cesium excited state population, which is the same for both channels (the theoretical curves were displaced only to show that both channels predict the same behavior).

5.7 System Li–Cs

Schlöder and co-workers [14] have measured $\beta'_{\mathrm{Cs-Li}}$ and $\beta'_{\mathrm{Li-Cs}}$ and have associated these loss rates with the Li−Cs* channel (Figs. 11a and 11b). They observed that $\beta'_{\mathrm{Cs-Li}}$ increases strongly as the lithium detuning, Δ_{Li}, increases. But such observation can not be explained by the Li−Cs* channel. Because in this channel, neither the cesium escape velocity or the cesium excited state population depend on the lithium detuning, but only on the cesium detuning. To explain this observation, they rely on the velocity between Li and Cs atoms with depends on the Δ_{Li}, and a good agreement is observed. We have compared their results with our model consider radiative escape in the Li−Cs* channel, and the theoretical prediction is shown in Figure 11a (full line) for $\beta'_{\mathrm{Cs-Li}}$. The agreement is reasonable, and the observed minimum is due to the fact that there is a maximum in the Cs trap depth as a function of Δ_{Cs}, which reflects into the trap loss rate as a minimum. In Figure 11b, we show the experimental results for $\beta'_{\mathrm{Li-Cs}}$ as a function of Δ_{Li}. The theoretical prediction, considering the radiative escape in the Li−Cs* channel, is shown in Figure 11b as a full line for $\beta'_{\mathrm{Li-Cs}}$. The agreement is good, and the observed increase as a function of the Δ_{Li} is due to the decrease in the Li trap depth.

5.8 Cross species trap loss rate as a function of mass

After undergoing the collision, the atoms of an atomic pair will share the energy released (ΔE), depending on their mass. If fact, the energy (ΔE_A) gained by A atom is given as $\Delta E_A = \Delta E(m_A/m_{eq})$, where $m_{eq} = m_A(1 + m_A/m_B)$ (equivalent mass). If the mass of A atom decreases, the amount of energy gained by it will increase and the A atom will get most of the released energy. Using the experimental results presented here, we plotted the heteronuclear trap loss rate (β') for Li, Na and Rb due to collisions with Cs (Fig. 12a); and the heteronuclear trap loss rate (β') for Na, K and Cs due to collisions with Rb (Fig. 12b) as a function of the equivalent mass (m_{eq}). The solid circles represent the experimental results and the open circles the theoretical prediction considering only the excited-ground channel (in fact excited-excited channel presents the same mass dependence). We should point out that for each colliding pair, we used the respectively C_6 and escape velocity. In Figure 12a we observe a very good agreement between theory and experiment when one of the colliding partners is a Cs atom. And the observed dependence is due to the fact that as the other partner gets lighter it will get most of the released energy, and therefore its loss rate will be larger. In Figure 12b, there is disagreement between theory and experiment when one of the colliding partners is rubidium atom. The disagreement is very clear for the case of K−Rb system, and this system is particular interesting because its theoretical C_6 [29] is about one order of magnitude larger than the others, and our theoretical model is very sensitive to such parameter. This disagreement still remains to be investigated theoretically.

6 Conclusions

To summarize, we presented a review on the heteronuclear trap loss rate measured for the Na−K, Na−Rb, Na−Cs, K−Rb, Rb−Cs, and Li−Cs systems. We also presented the heteronuclear trap loss rate for the Cs−K system for the first time. We should point out that there is some recent preliminary experiments in other mixtures, such as LiNa [41] and ArRb [42]. In the high intensity regime we concluded that Radiative Escape is the main loss process for most of the systems. A model, based on the GP model, was implemented for the A*–B and A*–B* channels and

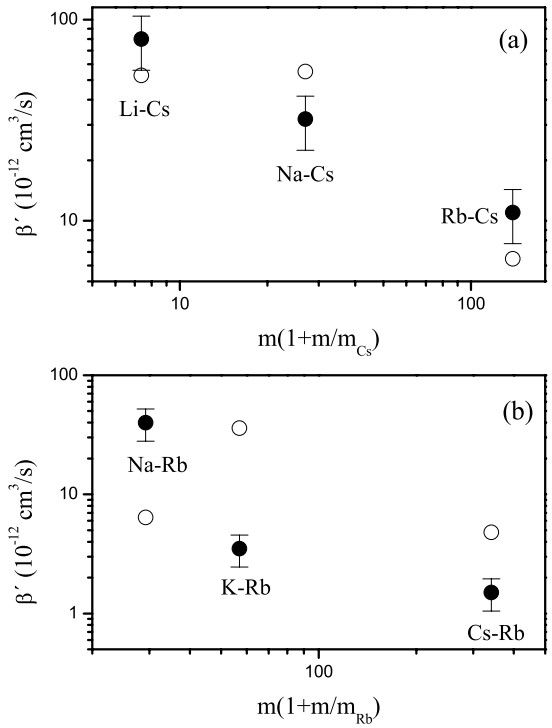

Fig. 12. Experimental results for the trap loss rates β' observed in different species (a) in the presence of ^{133}Cs, (b) in the presence of ^{85}Rb. The hollow circles represents the model's prediction considering only the channel A–B*. The experimental conditions were: (i) Li: $I = 47$ mW/cm^2 and $\Delta_{\rm Li} = -\Gamma_{\rm Li}$, (ii) Rb: $I = 170$ mW/cm^2 and $\Delta_{\rm Rb} = -\Gamma_{\rm Rb}$, (iii) Na: $I = 107$ mW/cm^2 and $\Delta_{\rm Na} = -\Gamma_{\rm Na}$, (iv) Na: $I = 10$ mW/cm^2 and $\Delta_{\rm Na} = -\Gamma_{\rm Na}$, (v) K: $I = 70$ mW/cm^2 and $\Delta_{\rm K} = -7\Gamma_{\rm K}$, (vi) Cs: $I = 400$ mW/cm^2 and $\Delta_{\rm Cs} = -\Gamma_{\rm Cs}$.

compared with the experimental results with good agreement. It is important to point out that the models are very sensitive to escape velocity. It is important to understand and to control such collisional processes in order to obtain atomic samples with high density/number of trapped atoms. These results are crucial for future experiments involving spectroscopy of the heteronuclear bound states and two Bose-Einstein condensation species. For the heavy atoms systems, the cross species trap loss rate do not introduce severe limitations for the combined species MOT, which is necessary for the magnetic trapping of two atomic species. In this sense, the results here presented are very useful. This information was also useful for the observation of heteronuclear molecules which were detected recently in the KRb system as well as in the RbCs system [43].

This work is supported by **FAPESP** (Fundação de Amparo à Pesquisa do Estado de São Paulo), **Pronex** (Programa de Núcleos de Excelência em Óptica Básica e Aplicada), and **Finep** (Financiadora de Estudos e Projetos). We also thanks Wanius Gracia and Leandro S. Aguiar for technical help.

References

1. J. Weiner, V.S. Bagnato, S.C. Zilio, P.S. Julienne, Rev. Mod. Phys. **71**, 1 (1999)
2. E. Raab, M. Prentiss, A. Cable, S. Chu, D. Pritchard, Phys. Rev. Lett. **59**, 2631 (1987)
3. W. Ketterle, K.B. Davis, M.A. Joffe, A. Martin, D. Pritchard, Phys. Rev. Lett. **70**, 2253 (1993)
4. E. Tiesinga, A. Moerdijk, B. Verhaar, H. Stoof, Phys. Rev. A **46**, R1167 (1992)
5. M.H. Anderson, J.R. Ensher, M.R. Matthews, C.E. Wieman, E.A. Cornell, Science **269**, 198 (1995); K.B. Davis, M.-O. Mewes, M.R. Andrews, N.J. van Druten, D.S. Durfee, D.M. Kurn, W. Ketterle, Phys. Rev. Lett. **75**, 3969 (1995)
6. M.S. Santos, A. Antunes, P. Nussenzveig, J. Flemming, S.C. Zílio, V.S. Bagnato, Laser Phys. **8**, 880 (1998); D. Sesko, T. Walker, C. Monroe, A. Gallagher, C. Wieman, Phys. Rev. Lett. **63**, 961 (1989); N.W.M. Ritchie, E.R.I. Abraham, Y.Y. Xiao, C.C. Bradley, R.G. Hulet, P.S. Julienne, Phys. Rev. A **51**, R890 (1995); J. Kawanaka, K. Shimizu, H. Takuma, F. Shimizu, Phys. Rev. A **48**, R883 (1993)
7. R.S. Williamson III, T. Walker, J. Opt. Soc. Am. B **12**, 1393 (1995); M.G. Peters, D. Hoffmann, J. Tobiason, T. Walker, Phys. Rev. A **50**, R906 (1994); D. Hoffmann, P. Feng, T. Walker, J. Opt. Soc. Am. B **11**, 712 (1994); C. Wallace, T. Dinneen, K. Tau, T. Grove, P. Gould, Phys. Rev. Lett. **69**, 897 (1992); M. Prentiss, A. Cable, J.E. Bjorkholm, S. Chu, E.L. Raab, D.E. Pritchard, Opt. Lett. **13**, 452 (1988); L.G. Marcassa, V.S. Bagnato, Y. Wang, C. Tsao, J. Weiner, O. Dulieu, Y.B. Band, P.S. Julienne, Phys. Rev. A **47**, R4563 (1993)
8. Tin-Lun Ho, V.B. Shenoy, Phys. Rev. Lett. **77**, 3276 (1996); H. Pu, N.P. Bigelow, Phys. Rev. Lett. **80**, 1130 (1998)
9. H. Wang, W.C. Stwalley, J. Chem. Phys. **108**, 5767 (1998)
10. G. Modugno et al., Science **294**, 1320 (2001); G. Roati, F. Riboli, G. Modugno, M. Inguscio, Phys. Rev. Lett. **89**, 150403 (2002)
11. G. Modugno et al., Science **297**, 2240 (2002); Z. Hadzibabic et al., Phys. Rev. Lett. **88**, 160401 (2002)
12. M.S. Santos, P. Nussenzveig, L.G. Marcassa, K. Helmerson, J. Flemming, S.C. Zílio, V.S. Bagnato, Phys. Rev. A **52**, R4340 (1995)
13. G.D. Telles, L.G. Marcassa, S.R. Muniz, S.G. Miranda, A. Antunes, C. Westbrook, V.S. Bagnato, Phys. Rev. A **59**, R23 (1999)
14. U. Schlöder, H. Engler, S. Schünemann, R. Grimm, M. Weidemüller, Eur. Phys J. D **7**, 331 (1999)
15. J.P. Shaffer, W. Chalupczak, N.P. Bigelow, Phys. Rev. A **60**, R3365 (1999)
16. L.G. Marcassa, G.D. Telles, S.R. Muniz, V.S. Bagnato, Phys. Rev. A **63**, 013413 (2001)
17. G.D. Telles, W. Garcia, L.G. Marcassa, V.S. Bagnato, D. Ciampini, M. Fazzi, J.H. Müller, D. Wilkowski, E. Arimondo, Phys, Rev. A **63**, 033406 (2001)
18. Y.E. Young, R. Ejnisman, J.P. Shaffer, N.P. Bigelow, Phys. Rev. A **62**, 055403 (2000)
19. A. Gallagher, D.E. Pritchard, Phys. Rev. Lett. **63**, 957 (1989)
20. A. Gallagher, Phys. Rev. A **44**, 4249 (1991)

21. A. Fioretti, J.H. Müller, P. Verkerk, M. Allegrini, E. Arimondo, P.S. Julienne, Phys. Rev. A **55**, R3999 (1997)
22. L.G. Marcassa, R.A.S. Zanon, S. Dutta, J. Weiner, O. Dulieu, V.S. Bagnato, Eur. Phys. J. D **7**, 317 (1999)
23. M.W. Mancini, A.L. de Oliveira, K.M.F. Magalhães, V.S. Bagnato, L.G. Marcassa, Eur. Phys. J. D **13**, 317 (2001)
24. R.J. Cook, Phys. Rev. A **20**, 224 (1979)
25. V.S. Bagnato, L.G. Marcassa, S.R. Miranda, S.R. Muniz, A.L. Oliveira, Phys. Rev. A **62**, 13404 (2000); S.R. Muniz, K.M.F. Magalhães, Ph. W. Courteille, M.A. Perez, L.G. Marcassa, V.S. Bagnato, Phys. Rev. A **65**, 015402 (2002)
26. N.W.M. Ritchie, E.R.I. Abraham, R.G. Hulet, Laser Phys. **4**, 1066 (1994)
27. L. G. Marcassa et al., Phys. Rev. Lett. **61**, 935 (1994)
28. V. Sanchez-Villicana, S.D. Gensemer, P. Gould, Phys. Rev. A **54**, R3730 (1996)
29. M.S. Santos, A. Antunes, P.S.P. Cardona, P. Nussenzveig, V.S. Bagnato, Phys. Rev. A **60**, 3892 (1999)
30. M.G. Peters, D. Hoffmann, J. Tobiason, T. Walker, Phys. Rev. A **50**, R906 (1994); D. Hoffmann, P. Feng, T. Walker, J. Opt. Soc. Am. B **11**, 712 (1994)
31. G.D. Telles, L.S. Aguiar, L.G. Marcassa, V.S. Bagnato, Phys. Rev. A **66**, 025403 (2002)
32. G.D. Telles, V.S. Bagnato, L.G. Marcassa, Phys. Rev. Lett. **86**, 4469 (2001)
33. B. Bussery, Y. Achkar, M. Aubert-Frécon, Chem. Phys. **116**, 319 (1987); M. Marinescu, H.R. Sadeghpour, Phys. Rev. A **59**, 390 (1999)
34. E.R.I. Abraham, W.I. MacAlexander, C.A.S. Sacket, R.G. Hullet, Phys. Rev. Lett. **74**, 1315 (1995); E.R.I. Abraham, W.I. MacAlexander, J.M. Gerton, R.G. Hullet, Phys. Rev. A **55**, R3299 (1997); J.R. Gardner, A. Cline, J.D. Miller, D.J. Heinzen, H.M.J.M. Boesten, B.J. Verhaar, Phys. Rev. Lett. **74**, 3764 (1995); E. Tiesinga, C.J. Williams, P.S. Julienne, K.M. Jones, P.D. Lett, W.D. Phillips, J. Res. Natl. Inst. Stand. Technol. **101**, 505 (1996); J.P. Burke Jr, C.H. Greene, J.L. Bohn, H. Wang, P.L. Gould, W.C. Stwalley, Phys. Rev. A **60**, 4417 (1999)
35. G. Ferrari, M. Inguscio, W. Jastrzebski, G. Roati, A. Simoni, Phys. Rev. Lett. **89**, 053202 (2002)
36. A. Fioretti, D. Comparat, A. Crubellier, O. Dulieu, F. Masnou-Seeuws, P. Pillet, Phys. Rev. Lett. **80**, 4402 (1998)
37. T. Takekoshi, B.M. Patterson, R.J. Knize, Phys. Rev. A **59**, R5 (1999)
38. C. Gabbanini, A. Fioretti, A. Lucchesini, S. Gozzini, M. Mazzoni, Phys. Rev. Lett. **84**, 2814 (2000)
39. A.N. Nikolov, J.R. Ensher, E.E. Eyler, H. Wang, W.C. Stwalley, P.L. Gould, Phys. Rev. Lett. **84**, 246 (2000)
40. F.K. Fatemi, K.M. Jones, P.D. Lett, E. Tiesinga, Phys. Rev. A **66**, 053401 (2002)
41. W. Wippel, C. Binder, L. Windholz, Eur. Phys. J. D **21**, 101 (2002)
42. C.I. Sukenik, H.C. Busch, Phys. Rev. A **66**, 051402 (2002)
43. M.W. Mancini et al., Phys. Rev. Lett. **92**, 133203 (2004); A.J. Kerman et al., Phys. Rev. Lett. **92**, 033004 (2004)